PolyPublie
Polytechnique Montréal

POLYTECHNIQUE MONTRÉAL
UNIVERSITÉ D'INGÉNIERIE

Titre: Title:	Failure analysis of a 316L stainless steel femoral orthopedic implant
Auteurs: Authors:	Benjamin Gervais, Aurelian Vadean, Maxime Raison, & Myriam Brochu
Date:	2016
Type:	Article de revue / Article
Référence: Citation:	Gervais, B., Vadean, A., Raison, M., & Brochu, M. (2016). Failure analysis of a 316L stainless steel femoral orthopedic implant. Case Studies in Engineering Failure Analysis, 5-6, 30-38. https://doi.org/10.1016/j.csefa.2015.12.001

Document en libre accès dans PolyPublie
Open Access document in PolyPublie

URL de PolyPublie: PolyPublie URL:	https://publications.polymtl.ca/4881/
Version:	Version officielle de l'éditeur / Published version Révisé par les pairs / Refereed
Conditions d'utilisation: Terms of Use:	CC BY-NC-ND

Document publié chez l'éditeur officiel
Document issued by the official publisher

Titre de la revue: Journal Title:	Case Studies in Engineering Failure Analysis (vol. 5-6)
Maison d'édition: Publisher:	Elsevier
URL officiel: Official URL:	https://doi.org/10.1016/j.csefa.2015.12.001
Mention légale: Legal notice:	

Ce fichier a été téléchargé à partir de PolyPublie, le dépôt institutionnel de Polytechnique Montréal
This file has been downloaded from PolyPublie, the institutional repository of Polytechnique Montréal

https://publications.polymtl.ca

Case Studies in Engineering Failure Analysis 5–6 (2016) 30–38

Contents lists available at ScienceDirect

Case Studies in Engineering Failure Analysis

journal homepage: www.elsevier.com/locate/csefa

Case study

Failure analysis of a 316L stainless steel femoral orthopedic implant

Benjamin Gervais [a,b,*], Aurelian Vadean [a], Maxime Raison [a,b], Myriam Brochu [a]

[a] Department of Mechanical Engineering, Polytechnique de Montréal, 2500 Chemin de Polytechnique, Montréal, QC, Canada H3T 1J4
[b] Research Centre, CHU Sainte-Justine, 3175 Chemin de la Côte-Sainte-Catherine, Montréal, QC, Canada H3T 1C4

ARTICLE INFO

Article history:
Received 10 September 2015
Received in revised form 3 December 2015
Accepted 17 December 2015
Available online 8 January 2016

Keywords:
Biomechanics
Fatigue
Fractographic analysis
Locking compression plate
Finite element analysis

ABSTRACT

This study presents a failure analysis of a femoral orthopedic implant. This implant is a locking compression plate that was fixed to a broken femur using two types of screws: locking and compression screws. The study elucidates the causes of an in situ premature failure of the plate and screws. Chemical analysis, hardness tests, and microstructural analysis confirmed that the implant was manufactured from cold-worked stainless steel 316L. The macro and micro fractographic analyses revealed that the failure mechanism was high-cycle fatigue and that the implant underwent approximately 10^6 loading cycles before failure. A finite element analysis of the assembly indicated that the crack initiation sites are located in the region where the highest stresses are observed. This numerical analysis confirmed that walking induces the loading condition needed for this specific failure. According to this loading condition and to the material properties, the stress amplitude that initiated and propagated the crack is estimated to be in the range of 400 MPa. Several considerations, both mechanical and medical, are discussed in order to explain the failure and to improve the system durability. From an engineering perspective, implant geometry and installation procedure could be optimized in order to reduce the stress concentrations that developed near the crack origin.
© 2016 The Authors. Published by Elsevier Ltd. This is an open access article under the CC BY-NC-ND license (http://creativecommons.org/licenses/by-nc-nd/4.0/).

1. Introduction

In orthopedic surgery, locking compression plates (LCP) are commonly used to stabilize fractured bone parts together. LCPs are generally manufactured with combi-holes that aim to accommodate two types of screws: locking and compression screws [1]. The choice of screws allows orthopedists to customize their installation method to balance compression and locking capability. This balance is necessary to provide angular stability and to limit the contact with the bone to preserve the blood supply and the tissue viability. Compression is known to produce the strain needed for the bone during the healing process of reconstruction [1]. Even though LCPs show uncontradicted advantages for healing fractured bones, their mechanical stability is technically difficult to maintain [2]. In 2003, a study involving 130 fractures repaired with a LCP

Abbreviations: LCP, Locking compression plate; SEM, Scanning electron microscope; HRC, Rockwell hardness scale; ASTM, American society for testing and materials; ASM, American society for metals; FEA, Finite element analysis.

* Corresponding author at: Research Centre, CHU Sainte-Justine, 3175 Chemin de la Côte-Sainte-Catherine, Montréal, QC, Canada, H3T 1C4. Tel.: +1 5143741710 x8639.

E-mail addresses: benjamin.gervais@polymtl.ca (B. Gervais), aurelian.vadean@polymtl.ca (A. Vadean), maxime.raison@polymtl.ca (M. Raison), myriam.brochu@polymtl.ca (M. Brochu).

http://dx.doi.org/10.1016/j.csefa.2015.12.001
2213-2902/© 2016 The Authors. Published by Elsevier Ltd. This is an open access article under the CC BY-NC-ND license (http://creativecommons.org/licenses/by-nc-nd/4.0/).

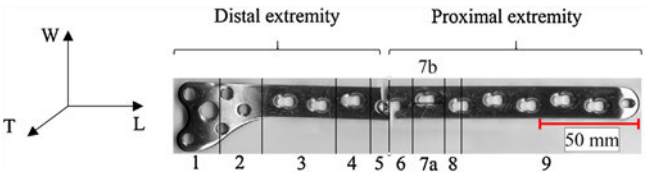

Fig. 1. Broken implant with the numbering used in this investigation. Axes system is defined by *L*: length, *W*: width and *T*: thickness.

showed 27 complications, with 18 of them requiring a second intervention [3]. The most common complications were non-union of the bone, loosening of the implant, breakage of the implant or an additional bone fracture. The objective of this study is to understand the failure mechanism of a specific LCP that failed prematurely.

The studied system is composed of a LCP fixed to a broken femur using both locking and compression screws. A picture of the broken implant is shown in Fig. 1. The distal extremity is situated closer to the knee and on the opposite side, the proximal extremity is closer to the hip. The failure analysis of the LCP was performed in 3 steps: material characterization (Section 4.1), fractographic analysis (Section 4.2), and preliminary finite element analysis (FEA) of the stresses seen by the implant (Section 5). A discussion explaining the failure mechanism and the root causes of failure is proposed in Sections 6 and 7.

2. Circumstances of failure

The implant studied is a 242 mm long plate with 10 combi-holes (Fig. 1). It was installed on the distal left femur of a male patient. The same type of implant was also installed on the proximal extremity of the tibia, since the patient additionally suffered from a tibia fracture. This second implant, which remained intact, is not investigated in the present study. The postoperative LCP installation of the femoral implant is shown on the radiograph of Fig. 2a. A total of 3 locking screws (LS) and 2 compression screws (CS) were used to fix the implant to the femur proximal extremity. Following an unexpected fall of the patient, the system failure was revealed by radiography, as shown in Fig. 2b. Removal of the implant confirmed the implant failure and the failure of one locking screw (LS#3) and one compression screw (CS#1). The postoperative incident occurred less than 2 years after the initial surgery.

3. Experimental procedure

According to the provided information, the plate was manufactured from 316L stainless steel [4]. Chemical analysis, metallographic observations and hardness tests were performed to validate this information. The plate was first cut into samples according to the schematic drawn in Fig. 1. An optical spectrometric analysis of sample #2, based on ASTM E1086-08 [5], was conducted to characterize the implant chemistry. Sample #7a was polished and etched with a solution composed of 150 mL of distilled water, 50 mL of HCl and 50 mL of HNO_3, for 90 s to reveal the material microstructure. Sample #7b was used to perform Rockwell C hardness measurements according to ASTM E18-15 [6]. The fracture surfaces were observed

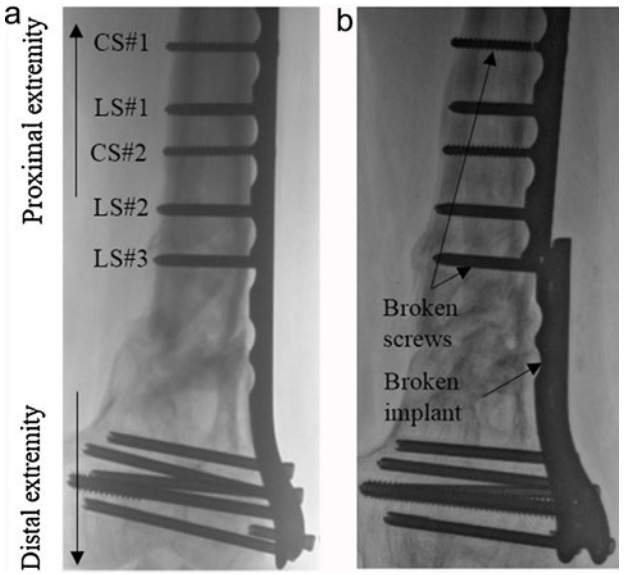

Fig. 2. Radiographies of the femur with the implant and screws (a) before and (b) after the failure.

using a binocular and a scanning electron microscope (SEM). Finally, a finite element analysis was performed using the Altair HyperWorks suite.

4. Experimental results

4.1. Material characterization

4.1.1. Chemical analysis

The measured chemical composition of the studied LCP is shown in the second column of Table 1. According to ASTM standard F138-13a [7], this composition meets the requirement for a 316L stainless steel, as shown in the third column of Table 1. 316L stainless steel is typically used to manufacture surgical implants [8].

4.1.2. Microstructural analysis

Stainless steel 316L has an austenitic microstructure. The grains observed in Fig. 3a are elongated in the longitudinal direction (L) of the implant indicating that the material was plastically deformed. The amount of plastic deformation could not be accurately evaluated from Fig. 3b, but a similar microstructure was found to characterize a 50% cold-worked state [8]. The amount of plastic deformation is necessary to give an estimation of the mechanical properties (see Section 4.1.3).

4.1.3. Mechanical properties

An average hardness of 33.4 HRC was measured. Such a hardness value characterizes 30–60% cold-worked 316L stainless steel [9]. Beside hardness, no mechanical properties were experimentally obtained because of the limited implant size. However, an estimation of the mechanical properties is proposed in Table 2 according to ASTM F138-13a [7] and to ASM Handbook [10].

Yield and tensile strengths are minimal values of mechanical properties given by the ASTM standard. The material studied could have higher strengths, according to typical values for 316L used in biomedical application [9].

According to ASM Handbook [10], the 10^7 cycles fatigue limit with a fully reverse loading conditions (stress ratio, $R = \sigma_{min}/\sigma_{max}$, equals to -1) is 256 MPa. The actual cyclic stress condition during walking is closer to a unidirectional loading, $R = 0$

Table 1
Chemical analysis of the implant material.

Elements	Mass content [%] (experimental)	Mass content [%] (ASTM F138 grade 316L)
Carbon (C)	0.028	≤0.030
Silicon (Si)	0.39	≤0.75
Manganese (Mn)	1.80	≤2.00
Phosphorus (P)	0.019	≤0.025
Sulfur (S)	0.002	≤0.010
Chromium (Cr)	17.52	17.00–19.00
Molybdenum (Mo)	2.64	2.25–3.00
Nickel (Ni)	14.76	13.00–15.00
Copper (Cu)	0.12	≤0.50
Iron (Fe)	Balance	Balance

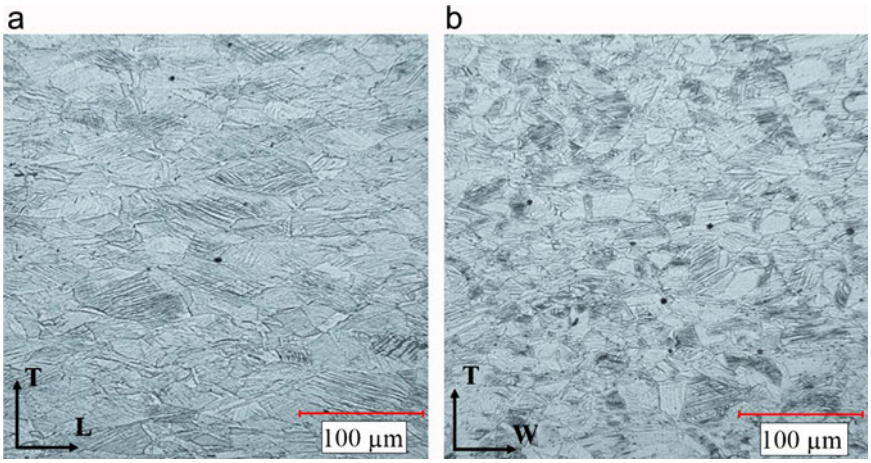

Fig. 3. Microstructure of the (a) longitudinal and (b) cross-sectional section of the studied implant at 200×.

Table 2
Mechanical properties of 316L stainless steel medical implant 50% cold-worked.

	Yield strength, S_y	Ultimate tensile strength, S_{ut}	Young's modulus, E	Fatigue limit for 10^7 cycles, $R = 0$, σ_{max}	Toughness, K_c
Minimum as per ASTM F138 [7]	690 MPa [7]	860 MPa [7]	–	–	–
Typical values from literature	1000 MPa [9]	1240 MPa [9]	192 GPa [10]	394 MPa [10]	112 MPa $m^{1/2}$ [10]

[11]. Therefore, a Goodman diagram was plotted to calculate the 10^7 fatigue limit at $R = 0$, which is $\sigma_{max} = 394$ MPa. These mechanical properties will be used to comment the finite element analysis performed in Section 5.

4.2. Failure analysis

4.2.1. Visual examination

Fig. 1 shows that the fracture occurred on a plane perpendicular to the implant L axis. Making the assumption that the crack propagated in mode I, this indicates that the principal stresses are longitudinal. The implant fracture surfaces are shown in Fig. 4a and b. Beach marks indicating the direction of crack propagation are visible on both surfaces, Fig. 4c and d. These features are specific to fatigue failure. Propagation lines are also visible and converge to the crack initiation site represented by a red dot. One can notice that fatigue initiated from the implant upper surface at the circumference of a combi-hole. The visual examination of the ruptured section (Fig. 4c) yields that the crack propagated by fatigue on more than 85% of the fracture surface, which corresponds approximately to the blue beach mark line. On the other side (Fig. 4d), beach marks were only observable on approximately 30% of the fracture surface. The broken screws fracture surfaces were also briefly analyzed, Fig. 4e and f. The presence of beach marks clearly indicated fatigue failure. This shows that both the implant and the screw failed progressively and over several loading cycles of low stress amplitude.

4.2.2. Scanning electron microscopy

Fig. 4g and h, respectively taken at 2 and 4.5 mm away from the initiation site of Fig. 4d, show fatigue striations. It confirms that the crack propagated trough the implant over nearly 85% of its thickness. The spacing between fatigue striations also gives an indication of the crack growth rate. The larger striation spacing in Fig. 4h (higher crack growth rate) confirms that the crack propagated from the upper surface toward the bone surface.

At crack initiation site, two surface discontinuities are observed (Fig. 4i). A thread root, also concentrating the stress, is observed at the bottom of Fig. 4i. Surprisingly, the crack did not initiate at the root of a thread or at the largest surface discontinuity. The propagation lines rather converge toward a smaller depression, less than 10 μm deep. It was not possible to confirm that this depression coincides to a contact point between the screw head and the implant. It has a size comparable to machining marks also observed on the inner surface of the compression hole.

5. Finite element analysis

The previous section presented the mechanical properties associated with the implant material and showed fatigue failure evidences by fractographic analysis. In Section 5, it will be attempted to precise the loading conditions responsible for failure with a finite element analysis.

Several orthopedic studies use finite element analysis to simulate the stresses in medical devices, such as for the intramedullary nail [12]. Some are comparing the efficiency of LCP versus nail [13,14] and others are proposing simple refinements of the geometrical aspects of the LCP [15]. Another study uses FEA results to suggest installation principles to better control the stability of the system [16]. In most of these simulations, the body weight is simply applied axially on the femur as an input. In the presented finite element analysis, more complex forces are input to simulate the stresses developed during a gait cycle. Loadings are based on a motion capture analysis performed in laboratory, as will be explained in Section 5.1.

5.1. Modeling and analysis

The geometry of the modeled system is represented in Fig. 5a–c. It is composed of 6 parts assembled together: the LCP along with its 8 locking screws (1 part), the 2 femur parts, and 3 compression screws.

The femur cortical bone is modeled as a cylinder with average human femur dimensions, i.e. 27 and 13 mm for the external and internal diameters respectively [17]. The cancellous part of the bone has not been modeled. It is represented by an empty area inside the cortical bone. The bone Young modulus (7 GPa) and Poisson's ratio (0.3) have been adopted from the results of flexion tests performed by Cristofolini et al. [18]. As far as the implant and screws properties are concerned, a Young Modulus, E, of 192 GPa, and a Poisson's ratio, υ, of 0.3 were used, which are typical of steel.

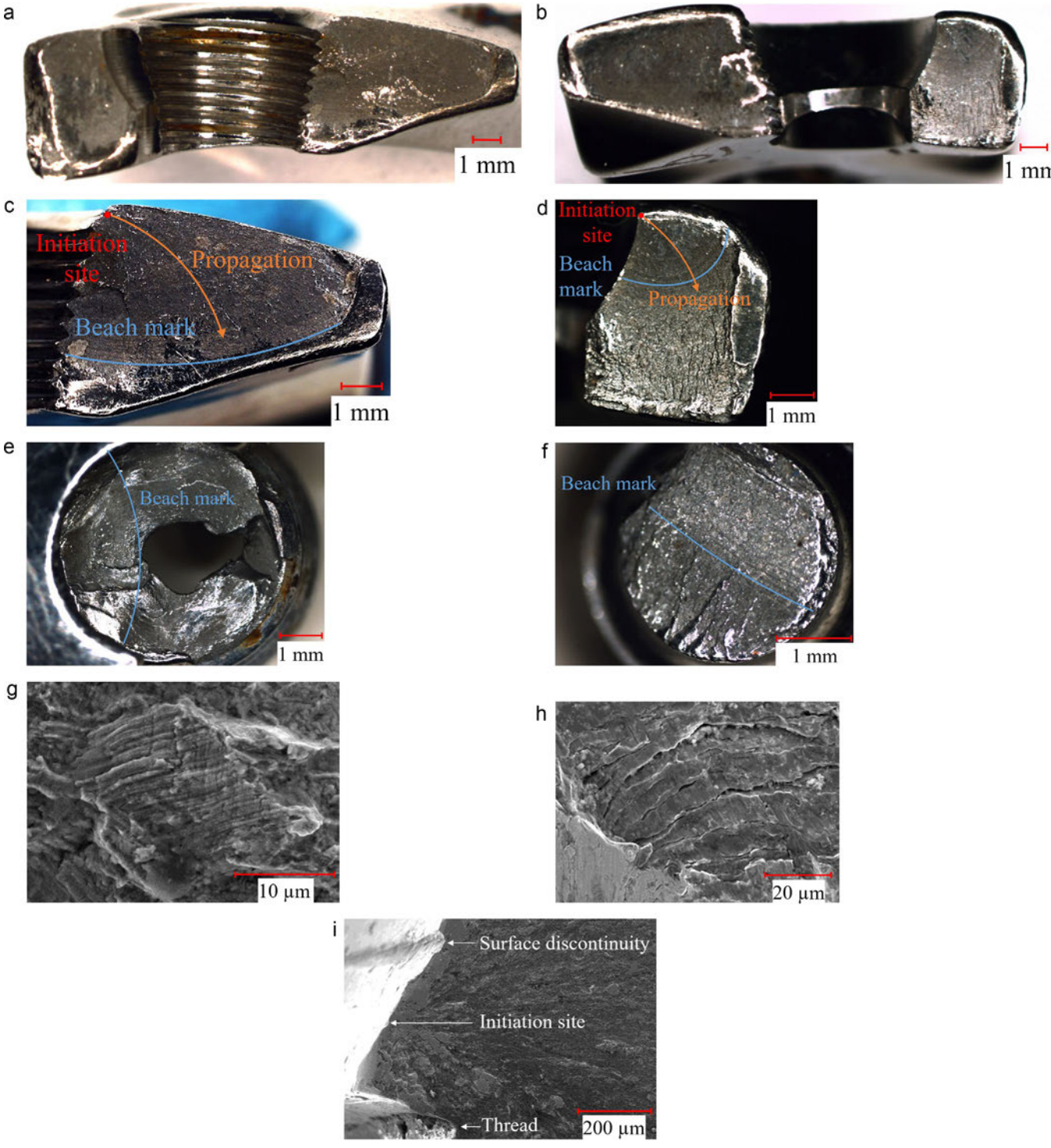

Fig. 4. Fracture surface on sample #5 (a) and on sample #6 (b). Beach marks observation of fracture surfaces on sample #5 (c) and sample #6 (d) at 6.7×. Beach marks observation of screw LS#3 (e) and CS#1 (f) at 20×. SEM photo of striations observed at (g) short and (h) long distance from the initiation site at 1500×. (i) SEM photo of a surface discontinuity and the initiation site at 150×.

The geometry of the bone and plate were meshed using 5 and 3 mm linear tetrahedral elements respectively (Fig. 5d). A refined mesh of 1 mm was applied in highly stressed regions to increase results accuracy. The screws were meshed using 2 mm hexahedral elements.

To simulate the action of the compression screws, a preload of 1000 N was applied in screws CS#1 and CS#2 which corresponds approximately to an installation torque of 4 N m. This installation torque is proposed by the manufacturer [4].

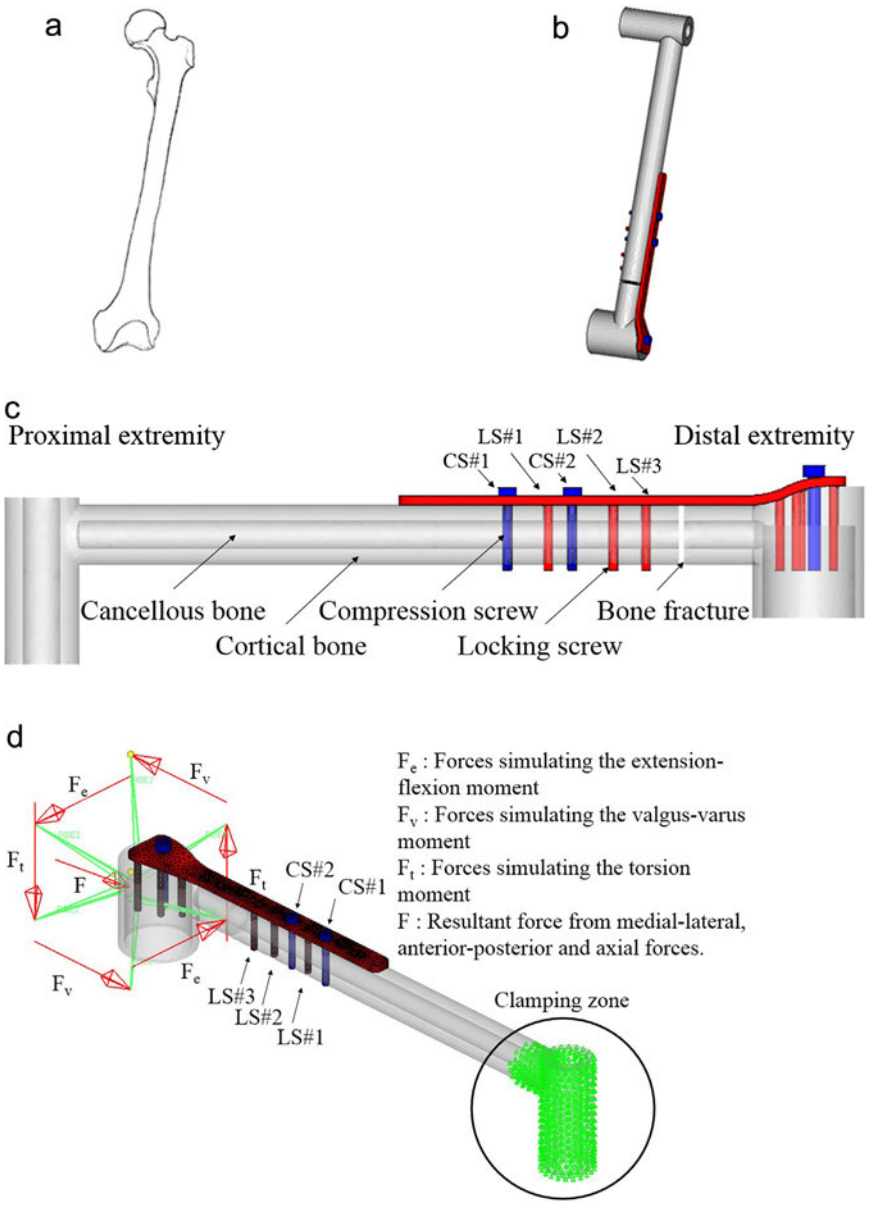

Fig. 5. Comparison between (a) a typical femur and (b) the finite element geometry of the femur and the implant. (c) Geometric modeling of the complete system. (d) Final mesh of the implant with loading conditions.

On the femur proximal extremity (hip region), boundary conditions of clamping were imposed (Fig. 5d) as previously used in the literature [13]. The working load itself (applied on the distal extremity) needed to be representative of the main activity performed by the patient between surgery and implant failure, which is walking. To obtain the characteristic loads and moments, a gait analysis of the patient was performed in the research laboratory of Marie Enfant rehabilitation center, equipped with a motion capture system composed of 12 cameras (T40S, Vicon-Oxford, UK). This analysis was approved by the Research Ethics Board of Ste-Justine Hospital (CÉR-CHU-SJ#4161). Results obtained were forces and moments at knee as a function of time during gait cycles. The average values over 3 cycles are comparable with results found in the literature [19]. The moments (M_e, M_v, M_t) and force (F) applied to the model are reported in Table 3. They characterize the maximum resultant moment and force recorded during the gait cycles. This typically occurs at 25% of a gait cycle. They were applied on the distal extremity of the femur, in the middle of the condyles with rigid bodies (knee region) as shown in Fig. 5d. The gait analysis confirmed that the minimum moments and forces are close to zero confirming the loading hypothesis $R = 0$, proposed in Section 4.1.3.

Table 3
Knee moments and force at 25% of gait cycle.

Extension-flexion moment, M_e	Valgus-varus moment, M_v	Torsion moment, M_t	Maximum resultant force, F
8 N m	35 N m	8 N m	607 N

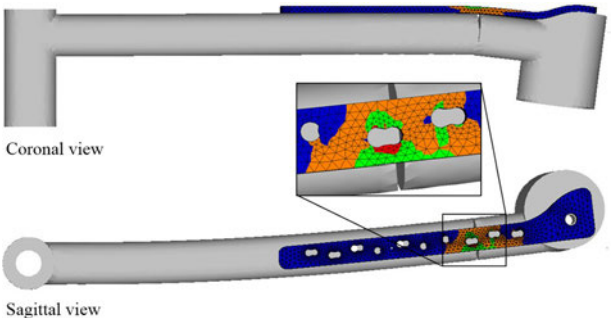

Fig. 6. Displacement (scale factor of 3) and Von Mises stress on the implant shown in the coronal and sagittal view.

5.2. Numerical results

After processing, the stresses distribution within the implant was obtained (Fig. 6). The maximum stress is located at the circumference of the hole closest to the bone fracture. Moreover, the stress is higher on the upper plate surface, which is specific to the bending load imposed. The displacement analysis demonstrates the effect of the bending moments in two planes: coronal and sagittal, shown by the two views of Fig. 6.

Surprisingly, the hole where the Von Mises stress is maximum is not the location where the crack initiation site was observed in the fractographic analysis of Section 4.2. Fig. 1 (real case) shows that the fracture occurred in the fourth combi-hole, whereas Fig. 6 (model) shows that the highest stress is in the third combi-hole, both counted from the distal extremity. This is probably due to the limitations of the finite element analysis. It was difficult to model the complex bone fracture and the boundary conditions of forces application. The latter should represent the muscle attachments to the bone, which was not considered in this preliminary finite element analysis.

From a general point of view, Fig. 6 still demonstrates that the failure occurred in a highly stress region. Moreover, the principal stress vector is parallel to the implant longitudinal axis which confirms mode I crack opening. Overall, this qualitative stress evaluation indicates that walking produces the necessary loading conditions to initiate and propagate a fatigue crack in the area close to the fracture. Nevertheless, further modeling considering nonlinear contacts between the parts and stress raisers such as threads is needed to quantitatively compare the finite element analysis with the material properties. A discussion on this topic is proposed in Section 6.

6. Description of the failure mechanism

The obtained results distinctly showed that the screws and the implant failed by fatigue. The fracture initiation site was properly identified by fractographic observations. The numerical analysis (FEA) demonstrated that walking alone creates a stress distribution that can explain crack initiation and propagation from the circumference of a hole.

In this section, the mechanical properties of stainless steel 316L (see Section 4.1.3) will be used to estimate the stress necessary to initiate the fatigue crack and to cause the implant final failure. The key mechanical properties used in these calculations are the maximum stress characterizing a fatigue life for 10^7 cycles at $R = 0$, $\sigma_{max} = 394$ MPa, and the material toughness, $K_c = 112$ MPa m$^{1/2}$. But before, the number of cycles that could have caused fatigue crack propagation will be established based on the patient activity in order to verify that failure occured in the high-cycle fatigue regime.

6.1. Number of cycles to failure

To support the crack initiation stress calculations based on the maximum stress at 10^7 cycles (see Section 6.2), the number of loading cycles (N) representative of the patient activity is first estimated. Knowing the elapsed time between implant installation and failure (2 years) and the type of activity (walking) a very simple calculation is proposed. According to Tudor-Locke et al. [20], the typical average number of steps during a day is 4,500 when the activities are restrained. This corresponds to 2,250 cycles per leg and sums up to 1,642,500 cycles if we consider that the patient walked every day during 2 years (2,250 cycle/day $\times$ 365 days/year $\times$ 2 years). This number is in the range of high-cycle fatigue but below 10^7 cycles as will be discussed in Section 6.2.

Table 4
Variables used in Newman and Raju equation for two symmetric corner cracks.

Variable	Description	Value	Unit
K_I	Stress-intensity factor (mode-I)	112 (= K_C at failure)	[MPa $m^{1/2}$]
S_t	Remote uniform tension stress	0	[MPa]
Q	Shape factor for elliptical crack	1.674	[-]
F	Boundary-correction factor	1.882	[-]
H	Bending multiplier	0.661	[-]
a, b, c, r and t	Geometrical dimensions	4, 9, 2.5, 2.5 and 5.3 x 10^{-3}	[m]
ϕ	Parametric angle of ellipse	0	[radian]

6.2. Crack initiation stresses

It was previously determined that the crack nucleated from the upper plate surface and propagated through the thickness under the effect of repeated bending stresses. The crack initiation stress can be approximated by a semi-log relationship of the type:

$$\sigma_{\max} = C + D\log(N), \tag{1}$$

where C and D are material constants. To calculate σ_{max} for 1,642,500 cycles using Eq. (1), failure at 0 cycle characterized by $\sigma_{max} = S_{ut\ min} = 860$ MPa and failure at 10^7 cycles characterized by $\sigma_{max} = 394$ MPa were used. The maximal stress (crack initiation stress) obtained using this methodology is 446 MPa. According to the hypothesis that walking caused fatigue failure, this should be the maximum stress developed during a gait cycle. To avoid fatigue crack initiation in the implant, the maximum cyclic stress should be below 394 MPa that characterizes "infinite" life.

6.3. Final failure stress

The final failure stress was also examined to evaluate if it is representative of walking or not. Based on the final crack size and on the material toughness, K_C, reported in Table 2 (112 MPa $m^{1/2}$), the remote bending stress that caused the component final failure (S_b) is calculated using Newman and Raju [21] Eq. (2) for two symmetric corner cracks at a hole:

$$K_I = (S_t + HS_b)\sqrt{\pi\frac{a}{Q}}F\left(\frac{a}{t},\frac{a}{c},\frac{r}{t},\frac{r}{b},\frac{c}{b},\phi\right), \tag{2}$$

with all the variables defined in Table 4.

It must be mentioned that Newman's equation is based on the hypothesis that the two surfaces on each side of the hole have the same area. Nevertheless, the failure surface studied is not fully symmetric as shown in Fig. 4a and b. The critical stress calculated, S_b, is 1040 MPa which is higher than the minimum ultimate tensile strength, $S_{ut\ min}$, of 860 MPa, but between the typical yield (1000 MPa) and tensile strength (1240 MPa) of the material. It is also much higher than the maximum stress characterizing a gait cycle. This indicates that the weakened section failed by tensile overload, which is consistent with the fact that the patient fell. The final failure of the implant was caused by a sudden overload.

7. Root causes of the failure

The analyzed fatigue failure was most probably caused by walking. This premature failure is the consequence of high-cycle fatigue. No hole surface or material discontinuity were observed at the crack initiation site. Nevertheless, the stresses developed during a gait cycle were apparently high enough to cause failure in less than 2 years. From an engineering point of view, the implant design and installation procedure could be reviewed to reduce the stress concentration.

The implant has numerous stress raisers. For a generic plate, disposing of many holes gives installation versatility to the surgeon but limits the load capacity of the system. Moreover, many holes are not used during the installation, but act as stress raisers when the implant is exposed to the loads.

In addition, the installation method seems to be only optimized according to medical purpose, such as the preservation of blood supply by limiting the contact pressure of the plate with the bone. This limits the preload applied on the screws which is detrimental to fatigue. It is well known that to fully protect a fastener from fatigue failure a prestress higher than the maximum cyclic stress should be applied [22]. Nevertheless the bone resistance must also be considered when choosing the preload. Poor bone condition can induce loosening of the screws and potentially increase the amplitude of the cyclic stresses.

The surgical point of view also needs consideration. The choice of the implant geometry and dimensions will affect the stresses. The plate span width, which corresponds to the ratio between the plate length and the fracture length, is a key parameter. For a comminuted fracture, the plate span width needs to be higher than 2 or 3 [23]. In the studied case, it is approximated 3, respecting the recommended value. The patient body mass index and its activity level are also parameters that could potentially affect the stresses and the failure mechanisms. The implant studied was installed on a patient with a

body mass index of 32.2 (North American average is in the range of 26.6) and with low level of activity since he was still recovering from a surgery.

Finally, the fall of the patient does not explain the premature implant failure even if the final failure occurred at this moment. An intact implant should have been able to sustain the exceptional loading caused by a fall. The failure occurred because of the weakened section due to high-cycle fatigue.

8. Conclusion and recommendations

The present work allowed describing the complex fatigue failure of a bone-LCP assembly. According to a finite element analysis and to an estimation of the number of fatigue cycles, walking was enough to induce fatigue damages. The stress variation needed to initiate and propagate the fatigue cracks within the screws and the implant were estimated to be in the range of 400 MPa *at R = 0*. The implant geometry and the uncontrolled preload are possible causes of stress concentration. Nevertheless, final failure was probably caused by the fall of the patient since the critical failure stress was higher than the minimum ultimate tensile strength, $S_{ut\ min}$ and close to the typical ultimate tensile strength, $S_{ut\ typ}$.

In future work, careful attention will be given to the geometric stress raisers characterizing the implant. It will be intent to propose a new implant design more resistant to fatigue without compromising the installation versatility. In addition, an extended study will be necessary to investigate if the bolting procedure can be improved in order to reduce the cyclic load amplitude experienced by the screws and plate. An optimization analysis accounting for the number of screws, their position and their preload are under development. The ideal installation scenario will then be proposed to practitioners to assist surgery.

Acknowledgements

The authors would like to acknowledge the Fonds de recherche du Québec – Nature et technologies (FRQNT), the Fondation de Polytechnique Montreal and the Unité de participation et d'initiation à la recherche (UPIR) of Polytechnique Montreal for sponsoring this research. The authors are grateful to M. Gregory Musy and Ms. Audrey Parent for their contributions to the finite element analysis and the gait analysis, respectively.

References

[1] Miller DL, Goswami T. A review of locking compression plate biomechanics and their advantages as internal fixators in fracture healing. Clin Biomech 2007;22:1049–62.
[2] Wood GCA, Naudie DR, McAuley J, McCalden RW. Locking compression plates for the treatment of periprosthetic femoral fractures around well-fixed total hip and knee implants. J Arthroplasty 2011;26:886–92.
[3] Sommer C, Gautier E, Müller M, Helfet DL, Wagner M. First clinical results of the Locking Compression Plate (LCP). Injury 2003;34(Suppl. 2):B43–54.
[4] Synthes. LCP Condylar Plate 4.5/5.0. Part of the LCP Periarticular Plating System; 2014.
[5] ASTM. Standard test method for optical emission vacuum spectrometric analysis of stainless steel by the point-to-plane excitation technique (E1086-08). In: ASTM Standards (03.05); 2008.
[6] ASTM. Standard test methods for Rockwell hardness of metallic materials (E18-15). In: ASTM Standards (03.01); 2015.
[7] ASTM. Standard specification for wrought 18chromium-14nickel-2.5molybdenum stainless steel bar and wire for surgical implants (F138-13a). In: ASTM Standards (13.01); 2013.
[8] Brunski JB. Metals basic principles. In: Biomaterials science: an introduction to materials in medicine. 3rd ed. Amsterdam: Academic Press; 2013. p. 111–27.
[9] Shetty RH, Ottersberg WH. Metals in orthopedic surgery. In: Encyclopedic handbook of biomaterials and bioengineering. New-York: CRC Press; 1995. p. 509–40.
[10] Narayan RJ. Medical application of stainless steels. ASM Handbook, vol. 23. Materials for Medical Devices, ASM International; 2012. p. 199–210.
[11] Pohler OEM. Failures of metallic orthopedic implants. ASM Handbook, vol. 11. Failure Analysis and Prevention, ASM International; 1986. p. 670–94.
[12] Cheung G, Zalzal P, Bhandari M, Spelt JK, Papini M. Finite element analysis of a femoral retrograde intramedullary nail subject to gait loading. Med Eng Phys 2004;26:93–108.
[13] Chen S-H, Chiang M-C, Hung C-H, Lin S-C, Chang H-W. Finite element comparison of retrograde intramedullary nailing and locking plate fixation with/without an intramedullary allograft for distal femur fracture following total knee arthroplasty. Knee 2014;21:224–31.
[14] Grujicic A, LaBerge M, Xie X, Arakere G, Pandurangan B, Grujicic M, et al. Computational investigation of the relative efficacies of nail-and plate-type proximal femoral-fracture fixation implants. Multidiscipl Model Mater Struct 2011;7:212–44.
[15] Anitha D, De SD, Sun KK, Doshi HK, Lee T. Improving stability of locking compression plates through a design modification: a computational investigation. Comput Methods Biomech Biomed Eng 2015;18:153–61.
[16] Stoffel K, Dieter U, Stachowiak G, Gächter A, Kuster MS. Biomechanical testing of the LCP – how can stability in locked internal fixators be controlled? Injury 2003;34(Suppl. 2):11–9.
[17] Croker SL, Clement JG, Donlon D. A comparison of cortical bone thickness in the femoral midshaft of humans and two non-human mammals. HOMO J Compar Hum Biol 2009;60:551–65.
[18] Cristofolini L, Viceconti M, Cappello A, Toni A. Mechanical validation of whole bone composite femur models. J Biomech 1996;29:525–35.
[19] Moisio KC, Sumner DR, Shott S, Hurwitz DE. Normalization of joint moments during gait: a comparison of two techniques. J Biomech 2003;36:599–603.
[20] Tudor-Locke C, Craig CL, Aoyagi Y, Bell RC, Croteau KA, De Bourdeaudhuij I, et al. How many steps/day are enough? For older adults and special populations. Int J Behav Nutr Phys Act 2011;8:80.
[21] Newman Jr , Raju IS. Stress-intensity factor equations for cracks in three-dimensional finite bodies subjected to tension and bending loads. Comput Methods Mech Fract 1986;311–34.
[22] Jensen WJ. Failures of mechanical fasteners. ASM Handbook, vol. 11. Failure Analysis and Prevention, ASM International; 1986. p. 529–49.
[23] Gautier E, Sommer C. Guidelines for the clinical application of the LCP. Injury 2003;34(Suppl. 2):63–76.